Surface Neural Networks

Anonymous Author(s)
Affiliation
Address
email

Abstract

In this paper we study data-driven representations for three-dimensional meshes, one of the prevalent objects used in Computer Graphics. Recent works have developed models that exploit the intrinsic geometry of manifolds and graphs, namely the Graph Neural Networks (GNNs) and its Spectral variants **??**, which learn from the local metric tensor via the Laplacian operator.

Despite offering excellent sample complexity and built-in invariances, intrinsic geometry alone fails to capture non-elastic local deformation phenomena, which is needed in many applications. In order to overcome this limitation, we propose several upgrades to GNNs that leverage the specific differential geometry properties of three-dimensional surfaces to increase their modeling power. In particular, we add extrinsic information to the input, and we exploit the Dirac operator, whose spectrum detects principal curvature directions, as opposed to the Laplace operator, which is only sensitive to mean curvature. We coin the resulting model the *Surface Neural Network (SNN)*.

We demonstrate the efficiency and versatility of SNNs on several challenging tasks: temporal prediction of mesh deformations under non-linear dynamics, generative models using a variational autoencoder framework with encoders and decoders given by SNNs, and shape correspondence.

1 Introduction

3D Computer Graphics is a field whose primary object of study are the representation, analysis, manipulation and synthesis of three-dimensional structures and its dynamics. Despite the vast amount of high-quality data available, data-driven approaches such as Deep Learning have yet to become mainstream. Contrary to Computer Vision, in which inputs are sampled on regular two or three-dimensional grids, the discretization of surfaces into meshes is adaptive, creating a challenge for traditional Convolutional Neural Network approaches.

Similarly as with CNNs when processing images or videos, one is interested in data-driven representations that strike the right balance between expressive power and sample complexity. In the case of CNNs, this is remarkably achieved by exploiting the inductive bias that most computer vision tasks are locally stable to deformations, leading to localized, multiscale features. In the case of surfaces and its discretized meshes, this creates a fundamental modeling choice between *extrinsic* versus *intrinsic* representations. Extrinsic representations rely on the specific embedding of surfaces within a three-dimensional ambient space, whereas intrinsic representations only capture geometric properties specific to the surface, irrespective of its parametrization. Whereas the former offer arbitrary representation power, they are unable to easily exploit stability priors.

Recently, the subfield *geometric deep learning* has emerged to provide data-driven intrinsic surface representations. Models based on Graph Neural Networks **?** and its Spectral variants **???** have been successfully applied to Computer Graphics tasks such as shape correspondence **?**. In its basic form, these models learn a deep representation over the discretized surface by combining a latent

Submitted to 31st Conference on Neural Information Processing Systems (NIPS 2017). Do not distribute.

representation at a given node with a local average of its neighboring latent representations, followed by a point-wise nonlinearity. Different models vary in their choice of local averaging and point-wise nonlinearity. By reparametrising the local smoothing with the original signal, one obtains the same model expressed in terms of the Laplacian operator, leading to the spectral interpretations.

Our present work fits into this line of work, by extending both the model and its applications. More specifically, we exploit the fact that surfaces in $\mathbb{R}^3$ admit a first-order differential operator, the *Dirac* operator, that is stable to discretization, provides a direct generalization of Laplacian-based propagation models and is able to detect principal curvature directions. By combining the Dirac operator with input coordinates we obtained a fully differentiable end-to-end feature representation that we apply to several challenging tasks.

First, we demonstrate the model efficiency on a temporal prediction task of complex dynamics, based on the ARAP (As Rigid As Possible) framework. Then we introduce a generative model for surfaces based on the variational autoencoder **??**.

Main contributions:

- Use of Dirac Operator.
- Generative Graph Neural Network model
- Temporal Prediction on Meshes under complex non-linear dynamics.

2 Related Work

- Geometric Deep Learning works: GNNs, Spectral nets, Hybrid versions (Chebyshev, Monet).
- Applications to mesh prediction: Bronstein. Monet paper.
- Physics prediction tasks: Battaglia et al, and MIT paper (ICLR'17).
- Guibas papers on point-cloud generation and shape segmentation.

3 Surface Neural Networks

This section presents our Surface Neural Network model and its basic properties. We start by introducing the problem setup and notations using the Laplacian formalism, and then introduce the Surface Neural Network model.

3.1 Laplacian Graph NNs

Our first goal is to define a trainable representation of discretized $\mathbb{R}^3$ surfaces. Let $\mathcal{M} = \{V, E, A\}$ be a triangular mesh, where $V = (v_i \in \mathbb{R}^3)_{i \leq N}$ contains the node coordinates, $E = (e_{i,j})$ corresponds to edges, and A is the triangulation. Since $\mathcal{M}$ can be cast as a discretization of a smooth manifold $S_{\mathcal{M}}$, the Laplace-Beltrami operator on $S_{\mathcal{M}}$ admits a stable discretization into $\mathcal{M}$, for instance using the cotangent angles **?**, that we denote by Δ.

This operator can be interpreted as a local, linear high-pass filter in $\mathcal{M}$ that acts on signals $x \in \mathbb{R}^{|V| \times d}$ defined on the nodes of the mesh as a simple matrix multiplication $\tilde{x} = \Delta x$. By complementing Δ with an *all-pass* filter and learning generic linear combinations followed by a point-wise nonlinearity, we thus obtain a simple generalization of localized convolutional operators in $\mathcal{M}$ that update a feature map from layer k to layer $k+1$ using trainable parameters A_k and B_k:

$$x^{k+1} = \rho\left(A_k \Delta x^k + B_k x^k\right) \ , \ A_k, B_k \in \mathbb{R}^{d_{k+1} \times d_k} \ . \tag{1}$$

By noticing that the Laplacian itself can be written in terms of the graph weight similarity by diagonal renormalization, this model is a specific instance of the graph neural network **???** and a generalization of the spectrum-free Laplacian networks from **?**. As shown in these previous works, convolutional-like layers (1) can be combined with graph coarsening or pooling layers, although in our current work, since we are interested in tasks that require keeping the mesh resolution, we will not use them.

In contrast to general graphs, meshes also contain a low-dimensional Euclidean embedding that contains potentially useful information in many graphics tasks, despite being extrinsic and thus not

invariant to the global position of the surface. A simple strategy to strike a good balance between expressivity and invariance is to include the node canonical coordinates as input channels to the network: $x^1 := V \in \mathbb{R}^{|V|\times 3}$. One can verify **?** that

$$\Delta V = -2H\mathbf{n}\,, \tag{2}$$

where H is the mean curvature function and $\mathbf{n}(u)$ is the normal vector of the surface at point u. It results that the Laplacian Neural model (1) has access to mean curvature and normal information. As discussed previously, this strategy increases the expressive power of the model, at the expense of losing invariance in the representation. Feeding Euclidean embedding coordinates into graph neural network models is related to the use of generalized coordinates from **?**.

By cascading K layers of the form (1) we obtain a representation $\Phi_\Delta(\mathcal{M})$ that contains generic features at each node location. When the number of layers K is of the order of $\mathrm{diam}(\mathcal{M})$, the diameter of the graph determined by $\mathcal{M}$, then the network is able to propagate and aggregate information across the whole surface. On regular meshes, $\mathrm{diam}(\mathcal{M}) \simeq |V|$, but one can leverage the multigrid structure to reduce the number of layers to $\simeq \log|V|$ **?** if necessary.

Equation (2) illustrates that a Laplacian layer is only able to extract isotropic high-frequency information, corresponding to the mean variations across all directions. Although in general graphs there is no well-defined procedure to recover anisotropic local variations, in the case of surfaces some authors (**?** and references therein) have considered anisotropic extensions. We describe next a particularly simple procedure to increase the expressive power of the network using a related operator from quantuum mechanics: the Dirac Operator.

3.2 Dirac Surface Neural Networks

The Laplace-Beltrami operator Λ is a second-order differential operator, constructed as $\Lambda = -\mathrm{div}\nabla$ by combining the gradient (a first-order differential operator) with its adjoint, the divergence operator. In an Euclidean space, one has access to these first-order differential operators separately, enabling oriented high-pass filters. Inspired from **?**, let us describe how to recover first-order differential operators in a surface that are stable to discretization on meshes.

For convenience, we embed $\mathbb{R}^3$ to the imaginary quaternion space $\mathrm{Im}(\mathbb{H})$ (see Appendix for details). The Dirac operator is then defined as a matrix $D \in \mathbb{H}^{|F|\times|V|}$ that maps (quaternion) signals on the nodes to signals on the faces. In coordinates,

$$D_{f,j} = \frac{-1}{2|\mathcal{A}_f|} e_j\ ,\ f \in F, j \in V\ ,$$

where e_j is the opposing edge vector of node j in the face f, and $\mathcal{A}_f$ is the area, as illustrated in Fig. ?. using counter-clockwise orientations on all faces.

The Dirac operator provides first-order differential information and is sensitive to local orientations. Moreover, one can verify **?** that

$$D^*D = \Delta\ ,$$

where D^* is the adjoint operator of D in the quaternion space (see Appendix).

The Dirac operator can be used to define a new neural surface representation that alternates layers with signals defined over nodes with layers defined over faces. Given a d-dimensional feature representation over the nodes of the mesh, $x \in \mathbb{R}^{|V|\times d}$, we define a d'-dimensional mapping to a face representation as

$$y_l(f) = \rho\left(\sum_{j\in f} x(j)^T C_l e_j\right)\ ,\ l = 1\ldots d'\ ,\ f \in F\ , \tag{3}$$

where $C_l \in \mathbb{R}^{d\times 3}$, $l = 1\ldots, d'$ are trainable parameters. Similarly, we define the adjoint layer that maps back to a $\tilde{d}$-dimensional signal over nodes as

$$\tilde{x}_l(j) = \rho\left(B_l x(j) + \frac{3}{\sum_{f\in j}|\mathcal{A}_f|}\sum_{f\in j} y(f)^T D_l \overline{e_j}\right)\ ,\ l = 1\ldots\tilde{d}\ ,\ j \in V\ , \tag{4}$$

where $D_l \in \mathbb{R}^{d' \times 3}$, $B_l \in \mathbb{R}^d$, $l = 1 \ldots, \tilde{d}$ are trainable parameters. A surface Neural Network layer is thus determined by parameters $\{B, C, D\}$ using equations (3) and (4) to define $x^{k+1} \in \mathbb{R}^{V \times d_{k+1}}$. We denote by $\Phi_D(\mathcal{M})$ the mesh representation resulting from applying K such layers.

- Relationship to edge feature transforms of **?**. But here instead of lifting to edge signals, we lift to face signals. Why is this a better property? Orientability?
- Why is this useful? Capture geometric information beyond the mean variations. What properties can we capture with Dirac that cannot be captured with Laplace?

3.3 Stability of Surface NNs

Here we describe how the Surface NNs are geometrically stable, because surface deformations become additive noise under the model.

Given a surface $S \subset \mathbb{R}^3$ or mesh $\mathcal{M}$, and a smooth deformation field $\tau : \mathbb{R}^3 \to \mathbb{R}^3$, we are particularly interested in two forms of stability:

- Given a discrete mesh $\mathcal{M}$ and a certain non-rigid deformation τ acting on $\mathcal{M}$, we want to certify that $\|\Phi(\mathcal{M}) - \Phi(\tau(\mathcal{M}))\|$ is small if $\|\nabla\tau(\nabla\tau)^* - \mathbf{I}\|$ is small, i.e when the deformation is nearly rigid.
- Given two discretizations $\mathcal{M}_1$ and $\mathcal{M}_2$ of the same underlying surface, we would like to control $\|\Phi(\mathcal{M}_1) - \Phi(\mathcal{M}_2)\|$ in terms of the resolution of the meshes.

These stability properties are important in applications, since most tasks we are interested in are stable to deformation and to discretization. The following theorem shows that both Φ_Δ and Φ_D preserve stability to deformations and discretizations.

Theorem 3.1. *Let $\mathcal{M}$ be a N-node mesh and x, $x' \in \mathbb{R}^{|V| \times d}$ be input signals defined on the nodes. Assume the nonlinearity $\rho(\,\cdot\,)$ is non-expansive. Then*

(a)

$$\|\Phi_\Delta(\mathcal{M}; x) - \Phi_\Delta(\mathcal{M}; x')\| \leq \alpha \|x - x'\| \,, \tag{5}$$

where α depends only on the trained weights and the mesh.

(b) Let $|\tau|_\infty := \sup_u \|\nabla\tau(u)(\nabla\tau(u))^* - \mathbf{1}\|$, where $\nabla\tau(u)$ is the Jacobian matrix of $u \mapsto \tau(u)$.

$$\|\Phi_\Delta(\mathcal{M}; x) - \Phi_\Delta(\tau(\mathcal{M}); x)\| \leq \beta |\tau|_\infty \|x\| \,, \tag{6}$$

where β is independent of τ and x.

(c) Let x, x' be piece-wise polyhedral constant approximations of $\bar{x}(t)$, $t \in S$, on discretizations $\mathcal{M}$ and $\mathcal{M}'$ of S, and assume $\bar{x}$ is Lipschitz with constant β. If ϵ is an upper bound of the normal field uniform distance **?** *between $\mathcal{M}$ and S and $\mathcal{M}$ and S, then*

$$\|\Phi_\Delta(\mathcal{M}; x) - \Phi_\Delta(\mathcal{M}', x')\| \leq \epsilon\gamma \|\bar{x}\| \,, \tag{7}$$

where γ is independent of x and S.

This theorem gives a simple stability certificate of Laplace-based Surface Neural Network representations with respect to geometric deformations and additive noise. Property (a) is not specific to surface representations, and is a simple consequence of the non-expansive property of our chosen nonlinearities. The constant α is controlled by the product of ℓ_2 norms of the network weights at each layer and the norm of the discrete Laplacian operator. Property (b) is based on the fact that the Laplacian operator is itself stable to deformations, a property that depends on two key aspects: first, the Laplacian is localized in space, and next, that it is a high-pass filter and therefore only depends on relative changes in position. Finally, property (c) certifies that if we use as generator of the SNN an operator that is consistent as the mesh resolution increases, the resulting surface representation is also consistent.

One caveat of our analysis is that the constants α, β, γ appearing in our bounds depend upon the bandwidth parameter $\tilde{A}^{-1}$, which increases as size of the mesh increases. This corresponds to the fact that the Laplacian operator is unbounded in the limit of continuous manifolds, but our current

proof does not exploit the regularity of the incoming signals at each layer, which is controllable if one considers half (or full) rectifications as nonlinearities. This analysis is left for future work.

A specific setup that we use in experiments is to use as input signal the canonical coordinates of the mesh $\mathcal{M}$. In that case, an immediate application of properties (a) and (b) above yields the following corollary:

Corollary 3.2. *Denote $\Phi(\mathcal{M}) := \Phi_{\mathcal{M}}(V)$, where V are the node coordinates of $\mathcal{M}$. Then, if $A_1 = 0$,*

$$\|\Phi(\mathcal{M}) - \Phi(\tau(\mathcal{M}))\| \leq \kappa |\tau|_\infty . \tag{8}$$

We conclude this section by studying the geometric stability of the Dirac-based surface neural network. In that case, the network is also shown to be stable, but using a deformation metric that in that case is sensitive to rigid rotations.

Theorem 3.3. *Denote by $\widetilde{|\tau|}_\infty := \sup_u \|\nabla\tau(u) - \mathbf{1}\|$. Then the previous theorem is valid by replacing Φ_Δ with Φ_D and $|\tau|_\infty$ with $\widetilde{|\tau|}_\infty$.*

3.4 Spatio-Temporal Representations

One specific task we

?

4 Generative Surface Models

In this section we introduce a generative model for meshes approximating surfaces with Euler Characteristic 1.

State-of-the-art generative models for images, such as Generative Adversarial Networks **?**, Pixel autoregressive networks **?** or Variational Autoencoders **?**, exploit the locality and stationarity of natural images in their probabilistic models, in the sense that the model satisfies

$$p_\theta(x) \approx p_\theta(x_\tau) \tag{9}$$

by construction, where x_τ is a small deformation of a given input x. This property is obtained via encoders and decoders (or discriminators and generators in the case of GANs) with a deep convolutional structure.

In our setting, we intend to exploit similar geometric stability priors on $p(\mathcal{M})$, a density over the space of meshes that we wish to fit to the data. A convenient way to proceed is to use the surface neural network representations described in the previous section, and exploit their stability properties to deformations (see Section 3.3).

A mesh generative model contains two distinct sources of randomness: on the one hand, the randomness associated to the underlying continuous surface, which corresponds to shape variability; on the other hand, the randomness associated to the discretization of the surface. Whereas the former contains the essential semantic meaning, the latter is not informative, and to some extent independent of the shape identity.

In order to formalize this factorization property, we focus initially on meshes that can be represented as a depth map over an (irregular) 2D mesh, referred as *height-field* meshes in the literature. That is, a mesh $\mathcal{M} = (V, E, F)$ is expressed as $(\tilde{\mathcal{M}}, f(\tilde{\mathcal{M}})$, where $\tilde{\mathcal{M}} = (\tilde{V}, \tilde{E}, \tilde{F})$ is now a 2D mesh and

$$f \,:\, \tilde{V} \to \mathbb{R}$$

is a *depth*-map encoding the original node locations V, as shown in Figure 4.

In this work, we consider the variational autoencoder framework **??**. It considers a mixture model of the form

$$p(\mathcal{M}) = \int p_\theta(\mathcal{M} \mid h) p_0(h) dh \,, \tag{10}$$

where $h \in \mathbb{R}^S$ is a vector of latent variables. As observed by some authors **?**, mixture models such as (10) when modeling natural images suffer to recover high-frequency information. A possible explanation for that comes from the fact that variability due to geometric deformations is highly nonlinear

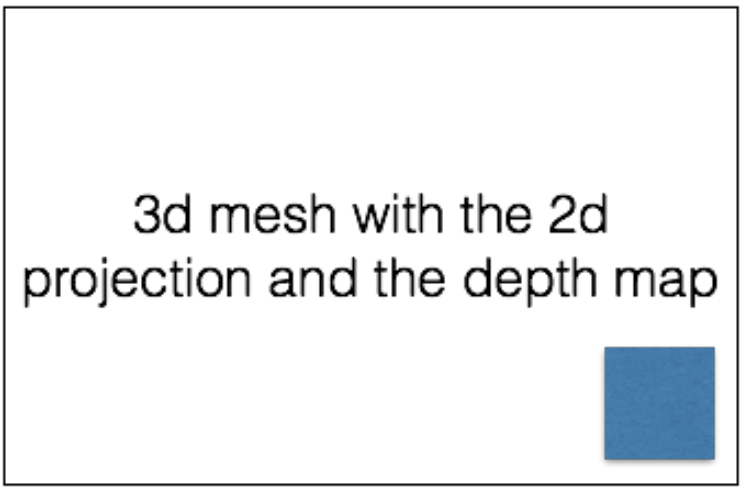

Figure 1: A 3D mesh $\mathcal{M}$ is expressed in terms of a "sampling" 2D irregular mesh $\tilde{\mathcal{M}}$ and a depth scalar field f over $\tilde{\mathcal{M}}$.

in the pixel space, and is therefore hard to describe with additive mixtures using unimodal likelihood terms $p_\theta(x \mid h)$ **?**. However, in surfaces, as described in Section 3.3, geometric deformations are additive perturbations on the node coordinates, making mixture models an appealing choice.

We thus consider a variational auto-encoder associated to model (10), which optimizes the variational lower bound of the data log-likelihood:

$$\min_{\theta,\psi} \frac{1}{L} \sum_{l \leq L} -\mathbb{E}_{h \sim q_\psi(h \mid \mathcal{M}_l)} \log p_\theta(\mathcal{M}_l \mid h) + D_{KL}(q_\psi(h \mid \mathcal{M}_l) \mid\mid p_0(h)) \; . \tag{11}$$

We thus need to specify a conditional generative model $p_\theta(\mathcal{M} \mid h)$, a prior distribution $p_0(h)$ and a variational approximation to the posterior $q_\psi(h \mid \mathcal{M})$, where θ and ψ denote respectively generative and variational trainable parameters. Based on the height-field representation, we choose for simplicity a separable model of the form

$$p_\theta(\mathcal{M} \mid h) = p_\theta(f \mid h, \tilde{\mathcal{M}}) \cdot p(\tilde{\mathcal{M}}) \; ,$$

where $\tilde{\mathcal{M}} \sim p(\tilde{\mathcal{M}})$ is a homogenous Poisson point process, and $f \sim p_\theta(f \mid h, \tilde{\mathcal{M}})$ is a Normal distribution with mean and isotropic covariance parameters given by a surface neural network:

$$p_\theta(f \mid h, \tilde{\mathcal{M}}) = \mathcal{N}(\mu(h, \tilde{\mathcal{M}}), \sigma^2(h, \tilde{\mathcal{M}})\mathbf{1}) \; , \text{ with } [\mu(h, \tilde{\mathcal{M}}), \sigma^2(h, \tilde{\mathcal{M}})] = \Phi_D(\tilde{M}; h) \; .$$

The generation step thus proceeds as follows. we first sample a 2D mesh $\tilde{\mathcal{M}}$ independent of the latent variable h, and then sample a depth field over $\tilde{\mathcal{M}}$ conditioned on h from the output of a decoder network $\Phi_D(\tilde{M}; h)$.

Finally, the variational family q_ψ is also a Normal distribution whose parameters are obtained from an encoder Surface Neural Network whose last layer is a global pooling that removes the spatial localization:

$$q_\psi(h \mid \mathcal{M}) = \mathcal{N}(\bar{\mu}, \bar{\sigma}^2\mathbf{1}) \; , \;\; \text{with} \;\; [\bar{\mu}, \bar{\sigma}] = \bar{\Phi}_D(\mathcal{M}) \; .$$

Comment on the limitations.

Generalization to other Euler Characteristic is immediate.

5 Experiments

A The Dirac Operator

spin transformations conformal maps quaternions.

B Further Numerical Experiments

C Proof of Theorem 3.1

C.1 Proof of (a)

We first show the result for the mapping $x \mapsto \rho\,(Ax + B\Delta x)$, corresponding to one layer of Φ_Δ. By definition, the Laplacian Δ of $\mathcal{M}$ is

$$\Delta = \mathrm{diag}(\bar{\mathcal{A}})^{-1}(D - W)\ ,$$

where $\bar{\mathcal{A}}_j$ is one third of the total area of triangles incident to node j, and $W = (w_{i,j})$ contains the cotangent weights **?**.

From **?** we verify that

$$\begin{aligned} \|D - W\| &\leq \sqrt{2}\max_j \left(d(j)^2 + \sum_{i\sim j} d(i) \right)^{1/2} \\ &\leq 2\sqrt{2}\sup_{i,j} w_{i,j} \sup_j S(j) \\ &\leq 2\sqrt{2}\cot(\alpha_{\min}) S_{\max}\ , \end{aligned} \tag{12}$$

where $S(j)$ denotes the number of neighbors of node j, $\alpha_{\min}$ is the smallest angle in the triangulation of $\mathcal{M}$ and $S_{\max}$ the largest number of incident triangles. It results that

$$\|\Delta\| \leq C\frac{\cot(\alpha_{\min})S_{\max}}{\inf_j \bar{\mathcal{A}}_j} := L_{\mathcal{M}}\ ,$$

which depends uniquely on the mesh $\mathcal{M}$ and is finite for non-degenerate meshes. Moreover, since $\rho(\,\cdot\,)$ is non-expansive, we have

$$\begin{aligned} \|\rho\,(Ax + B\Delta x) - \rho\,(Ax' + B\Delta x')\| &\leq \|A(x - x') + B\Delta(x - x')\| \\ &\leq (\|A\| + \|B\|L_{\mathcal{M}})\|x - x'\|\ . \end{aligned} \tag{13}$$

By cascading (13) across the K layers of the network, we obtain

$$\|\Phi(\mathcal{M}; x) - \Phi(\mathcal{M}; x')\| \leq \left(\prod_{k\leq K} (\|A_k\| + \|B_k\|L_{\mathcal{M}}) \right) \|x - x'\|\ ,$$

which proves (5).

C.2 Proof of (b)

To establish (6) we first observe that given three points $p, q, r \in \mathbb{R}^3$ forming any of the triangles of $\mathcal{M}$,

$$\|p - q\|^2(1 - |\tau|_\infty)^2 \leq \|\tau(p) - \tau(q)\|^2 \leq \|p - q\|^2(1 + |\tau|_\infty)^2 \tag{14}$$

$$\mathcal{A}(p, q, r)^2(1 - |\tau|_\infty C\alpha_{\min}^{-1} - o(|\tau|_\infty^2)) \leq \mathcal{A}(\tau(p), \tau(q), \tau(r))^2 \leq \mathcal{A}(p, q, r)^2(1 + |\tau|_\infty C\alpha_{\min}^{-1} + o(|\tau|_\infty^2)) \tag{15}$$

Indeed, (14) is a direct consequence of the lower and upper Lipschitz constants of $\tau(u)$, which are bounded respectively by $1 - |\tau|_\infty$ and $1 + |\tau|_\infty$. As for (15), we use the Heron formula

$$\mathcal{A}(p, q, r)^2 = s(s - \|p - q\|)(s - \|p - r\|)(s - \|r - q\|)\ ,$$

with $s = \frac{1}{2}(\|p-q\| + \|p-r\| + \|r-q\|)$ being the half-perimeter. By denoting s_τ the corresponding half-perimeter determined by the deformed points $\tau(p), \tau(q), \tau(r)$, we have that

$$s_\tau - \|\tau(p) - \tau(q)\| \leq s(1 + |\tau|_\infty) - \|p - q\|(1 - |\tau|_\infty) = s - \|p - q\| + |\tau|_\infty(s + \|p - q\|) \text{ and}$$

$$s_\tau - \|\tau(p) - \tau(q)\| \geq s(1 - |\tau|_\infty) - \|p - q\|(1 + |\tau|_\infty) = s - \|p - q\| - |\tau|_\infty(s + \|p - q\|)\ ,$$

and similarly for the $\|r-q\|$ and $\|r-p\|$ terms. It results that

$$\begin{aligned}\mathcal{A}(\tau(p),\tau(q),\tau(r))^2 &\geq \mathcal{A}(p,q,r)^2\left[1-|\tau|_\infty\left(1+\frac{s+\|p-q\|}{s-\|p-q\|}+\frac{s+\|p-q\|}{s-\|p-q\|}+\frac{s+\|p-q\|}{s-\|p-q\|}\right)-o(|\tau|^2)\right]\\ &\geq \mathcal{A}(p,q,r)^2\left[1-C|\tau|_\infty\alpha_{\min}^{-1}-o(|\tau|^2)\right]\ ,\end{aligned}$$

and similarly

$$\mathcal{A}(\tau(p),\tau(q),\tau(r))^2 \leq \mathcal{A}(p,q,r)^2\left[1+C|\tau|_\infty\alpha_{\min}^{-1}-o(|\tau|^2)\right]\ .$$

By noting that the cotangent Laplacian weights can be written (see Fig. ?) as

$$w_{i,j}=\frac{-\ell_{ij}^2+\ell_{jk}^2+\ell_{ik}^2}{\mathcal{A}(i,j,k)}+\frac{-\ell_{ij}^2+\ell_{jh}^2+\ell_{ih}^2}{\mathcal{A}(i,j,h)}\ ,$$

we have from the previous Bilipschitz bounds that

$$\tau(w_{i,j})\leq w_{i,j}\left[1-C|\tau|_\infty\alpha_{\min}^{-1}\right]^{-1}+2|\tau|_\infty\left[1-C|\tau|_\infty\alpha_{\min}^{-1}\right]^{-1}\left(\frac{\ell_{ij}^2+\ell_{jk}^2+\ell_{ik}^2}{\mathcal{A}(i,j,k)}+\frac{\ell_{ij}^2+\ell_{jh}^2+\ell_{ih}^2}{\mathcal{A}(i,j,h)}\right)\ ,$$

$$\tau(w_{i,j})\geq w_{i,j}\left[1+C|\tau|_\infty\alpha_{\min}^{-1}\right]^{-1}-2|\tau|_\infty\left[1+C|\tau|_\infty\alpha_{\min}^{-1}\right]^{-1}\left(\frac{\ell_{ij}^2+\ell_{jk}^2+\ell_{ik}^2}{\mathcal{A}(i,j,k)}+\frac{\ell_{ij}^2+\ell_{jh}^2+\ell_{ih}^2}{\mathcal{A}(i,j,h)}\right)\ ,$$

which proves that, up to second order terms, the cotangent weights are Lipschitz continuous to deformations.

Finally, since the mesh Laplacian operator is constructed as $\mathrm{diag}(\bar{\mathcal{A}})^{-1}(D-W)$, with $\bar{\mathcal{A}}_{i,i}=\frac{1}{3}\sum_{j,k;(i,j,k)\in F}\mathcal{A}(i,j,k)$, and $D=\mathrm{diag}(W\mathbf{1})$, let us show how to bound $\|\Delta-\tau(\Delta)\|$ from

$$\bar{\mathcal{A}}_{i,i}(1-\alpha_{\mathcal{M}}|\tau|_\infty-o(|\tau|^2))\leq\tau(\bar{\mathcal{A}}_{i,i})\leq\bar{\mathcal{A}}_{i,i}(1+\alpha_{\mathcal{M}}|\tau|_\infty+o(|\tau|^2)) \tag{16}$$

and

$$w_{i,j}(1-\beta_{\mathcal{M}}|\tau|_\infty-o(|\tau|^2))\leq\tau(w_{i,j})\leq w_{i,j}(1+\beta_{\mathcal{M}}|\tau|_\infty+o(|\tau|^2))\ . \tag{17}$$

Using the fact that $\bar{\mathcal{A}}$, $\tau(\bar{\mathcal{A}})$ are diagonal, and using the spectral bound for $k\times m$ sparse matrices from **?**, Lemma 5.12,

$$\|Y\|^2\leq\max_i\sum_{j;\,Y_{i,j}\neq0}|Y_{i,j}|\left(\sum_{r=1}^{l}|Y_{r,j}|\right)\ ,$$

the bounds (16) and (17) yield respectively

$$\begin{aligned}\tau(\bar{\mathcal{A}}) &= \bar{\mathcal{A}}(\mathbf{1}+\epsilon_\tau)\ ,\ \text{with}\ \|\epsilon_\tau\|=o(|\tau|_\infty)\ ,\text{and}\\ \tau(D-W) &= D-W+\eta_\tau\ ,\ \text{with}\ \|\eta_\tau\|=o(|\tau|_\infty)\ .\end{aligned}$$

It results that, up to second order terms,

$$\begin{aligned}\|\Delta-\tau(\Delta)\| &= \left\|\tau(\bar{\mathcal{A}})^{-1}(\tau(D)-\tau(W))-\bar{\mathcal{A}}^{-1}(D-W)\right\|\\ &= \left\|\left(\bar{\mathcal{A}}[\mathbf{1}+\epsilon_\tau]\right)^{-1}[D-W+\eta_\tau]-\bar{\mathcal{A}}^{-1}(D-W)\right\|\\ &= \left\|\left(\mathbf{1}-\epsilon_\tau+o(|\tau|_\infty^2)\right)\bar{\mathcal{A}}^{-1}(D-W+\eta_\tau)-\bar{\mathcal{A}}^{-1}(D-W)\right\|\\ &= \left\|\epsilon_\tau\Delta+\bar{\mathcal{A}}^{-1}\eta_\tau\right\|+o(|\tau|_\infty^2)\\ &= o(|\tau|_\infty)\ ,\end{aligned}$$

which shows that the Laplacian is stable to deformations in operator norm. Finally, by denoting $\tilde{x}_\tau$ a layer of the deformed Laplacian network

$$\tilde{x}_\tau=\rho(Ax+B\tau(\Delta)x)\ ,$$

it follows that

$$\begin{aligned}\|\tilde{x}-\tilde{x}_\tau\| &\leq \|B(\Delta-\tau(\Delta)x\| &(18)\\ &\leq C\|B\||\tau|_\infty\|x\|\ . &(19)\end{aligned}$$

Also,

$$\begin{aligned}\|\tilde{x} - \tilde{x'}_\tau\| &\leq \|A(x-x') + B(\Delta x - \tau(\Delta)x')\| \\ &\leq (\|A\| + \|B\|\|\Delta\|)\|x-x'\| + \|\Delta - \tau(\Delta)\|\|x\| \\ &\leq \underbrace{(\|A\| + \|B\|\|\Delta\|)}_{\delta_1}\|x-x'\| + \underbrace{C|\tau|_\infty}_{\delta_2}\|x\|\,,\end{aligned}$$

and therefore, by plugging (18) with $x' = \tilde{x}_\tau$, K layers of the Laplacian network satisfy

$$\begin{aligned}\|\Phi(x;\Delta) - \Phi(x;\tau(\Delta)\| &\leq \left(\prod_{j\leq K-1}\delta_1(j)\right)\|\tilde{x} - \tilde{x}_\tau\| + \left(\sum_{j<K-1}\prod_{j'\leq j}\delta_1(j')\delta_2(j)\right)|\tau\|_\infty\|x\| \\ &\leq \left[C\left(\prod_{j\leq K-1}\delta_1(j)\right)\|B\| + \left(\sum_{j<K-1}\prod_{j'\leq j}\delta_1(j')\delta_2(j)\right)\right]|\tau|_\infty\|x\|\,. \quad \square\,.\end{aligned}$$

C.3 Proof of (c)

This result is an immediate consequence of the consistency of the cotangent Laplacian to the Laplace-Beltrami operator on S **?**:

Theorem C.1 (**?**, Thm 3.4)**.** *Let $\mathcal{M}$ be a compact polyhedral surface which is a normal graph over a smooth surface S with distortion tensor $\mathcal{T}$, and let $\overline{\mathcal{T}} = (\det\mathcal{T})^{1/2}\mathcal{T}^{-1}$. If the normal field uniform distance $\|\overline{\mathcal{T}} - \mathbf{1}\|_\infty \leq \epsilon$, then*

$$\|\Delta_{\mathcal{M}} - \Delta_S\| \leq \epsilon\,. \tag{20}$$

Thus, given two meshes $\mathcal{M}$, $\mathcal{M}'$ approximating a smooth surface S in terms of uniform normal distance, and the corresponding irregular sampling x and x' of an underlying function $\bar{x} : S \to \mathbb{R}$, we have

$$\|\rho(Ax + B\Delta_{\mathcal{M}}x) - \rho(Ax' + B\Delta_{\mathcal{M}'}x')\| \leq \|A\|\|x-x'\| + \|B\|\|\Delta_{\mathcal{M}}x - \Delta_{\mathcal{M}'}x'\|\,. \tag{21}$$

Since $\mathcal{M}$ and $\mathcal{M}'$ both converge uniformly normally to S and $\bar{x}$ is Lipschitz on S, it results that

$$\|x - \bar{x}\| \leq \beta\epsilon\,,\ \text{and}\ \|x' - \bar{x}\| \leq \beta\epsilon\,,$$

thus $\|x - x'\| \leq 2\beta\epsilon$. Moreover, thanks to (20) we have

$$\|\Delta_{\mathcal{M}} - \Delta_{\mathcal{M}'}\| \leq 2\epsilon\,,$$

which from (21) results in

$$\begin{aligned}\|\rho(Ax + B\Delta_{\mathcal{M}}x) - \rho(Ax' + B\Delta_{\mathcal{M}'}x')\| &\leq 2\|A\|\beta\epsilon + \\ &\quad + \|B\|\|\Delta_{\mathcal{M}}x - \Delta_{\mathcal{M}'}x + \Delta_{\mathcal{M}'}x - \Delta_{\mathcal{M}'}x'\| \\ &\leq \epsilon\,(2\|A\|\beta + \|B\|\|x\|) + \|B\|\|\Delta_{\mathcal{M}'}\|\|x-x'\|\,,\end{aligned} \tag{22}$$

and therefore

$$\begin{aligned}\|\Phi_{\mathcal{M}}(x) - \Phi_{\mathcal{M}'}(x')\| &\leq \left(\prod_{k\leq K}\|B_k\|\|\Delta_{\mathcal{M}}\|\right)\|x-x'\| + \epsilon\left[\sum_{k\leq K}(2\|A_k\|\beta + \|B_k\|\|x\|)\prod_{k'\leq k}\|B_{k'}\|\|\Delta_{\mathcal{M}}\|\right] \\ &\leq \epsilon\left\{2\beta\left(\prod_{k\leq K}\|B_k\|\|\Delta_{\mathcal{M}}\|\right) + \left[\sum_{k\leq K}(2\|A_k\|\beta + \|B_k\|\|x\|)\prod_{k'\leq k}\|B_{k'}\|\|\Delta_{\mathcal{M}}\|\right]\right\}\,. \quad \square\,.\end{aligned}$$

D Proof of Corollary 3.2

$D_\tau S$ is linear: $D_\tau S = S + b(\tau)$, $\|\Delta b(\tau)\|$ small if $b(\tau)$ is smooth.

E Proof of Theorem 3.3